A&A 566, A121 (2014)
DOI: 10.1051/0004-6361/201322875


Astronomy & Astrophysics

# *XMM-Newton* and *Swift* observations of WZ Sagittae: spectral and timing analysis

A. A. Nucita[1,2], E. Kuulkers[3], F. De Paolis[1,2], K. Mukai[4,5], G. Ingrosso[1,2], and B. M. T. Maiolo[1,2]

[1] Department of Mathematics and Physics *E. De Giorgi*, University of Salento, via per Arnesano, CP 193, 73100 Lecce, Italy
e-mail: nucita@le.infn.it
[2] INFN, Sez. di Lecce, via per Arnesano, CP 193, 73100 Lecce, Italy
[3] European Space Astronomy Centre, SRE-O, PO Box 78, 28691 Villanueva de la Cañada (Madrid), Spain
[4] CRESST and X-ray Astrophysics Laboratory, NASA Goddard Space Flight Center, Greenbelt MD 20771, USA
[5] Department of Physics, University of Maryland Baltimore County, 1000 Hilltop Circle, Baltimore MD 21250, USA

Received 19 October 2013 / Accepted 19 April 2014

**ABSTRACT**

*Context.* WZ Sagittae is the prototype object of a subclass of dwarf novae with rare and long (super)outbursts, in which a white dwarf primary accretes matter from a low mass companion. High-energy observations offer the possibility of a better understanding of the disk-accretion mechanism in WZ Sge-like binaries.
*Aims.* We used archival *XMM-Newton* and *Swift* data to characterize the X-ray spectral and temporal properties of WZ Sge in quiescence.
*Methods.* We performed a detailed timing analysis of the simultaneous X-ray and UV light curves obtained with the EPIC and OM instruments on board *XMM-Newton* in 2003. We employed several techniques in this study, including a correlation study between the two curves. We also performed an X-ray spectral analysis using the EPIC data and *Swift*/XRT data obtained in 2011.
*Results.* We find that the X-ray intensity is clearly modulated at a period of ≃28.96 s, confirming previously published preliminary results. We find that the X-ray spectral shape of WZ Sge remains practically unchanged between the *XMM-Newton* and *Swift* observations. However, after correcting for interstellar absorption, the intrinsic luminosity is estimated to be $L_{\rm X}^{\rm Una} = (2.65 \pm 0.06) \times 10^{30}$ erg s$^{-1}$ and $L_{\rm X}^{\rm Una} = (1.57 \pm 0.03) \times 10^{30}$ erg s$^{-1}$ in 2003 and 2011, respectively. During the *Swift*/XRT observation, the observed flux is a factor ≃2 lower than that observed by *XMM-Newton* but is similar to the quiescent levels that are observed various times before the 2001 outburst.

**Key words.** binaries: general – white dwarfs – X-rays: binaries

## 1. Introduction

A cataclysmic variable (CV) is a binary system consisting of a white dwarf primary which accretes matter from a low mass companion via Roche lobe overflow (for a review, see Warner 1995). Systems with a primary with a relatively low magnetic field ($\lesssim 0.1$ MG) are expected to accrete via a Keplerian disk. In this case, half of the total potential gravitational energy is dissipated by the viscosity with the remainder being radiated away by the boundary layer. The spectral energy distribution emitted by the accretion disk peaks in the optical and ultraviolet bands, while the boundary layer radiates predominantly in the extreme ultraviolet and X-rays. Typical X-ray luminosities of CVs are in the range $10^{30}$–$10^{32}$ erg s$^{-1}$ (see, e.g., Lamb 1982; Baskill et al. 2005; Kuulkers et al. 2006). *XMM-Newton* (Jansen et al. 2001) is particularly useful for studying quiescent CVs as its large effective area allows us to detect faint sources in general and those during dips and eclipses in particular. Moreover, the possibility to observe the source simultaneously in the optical or ultraviolet (UV) bands with the optical monitor (OM) opens the possibility to study the correlations between light curves of the same source in different wavelengths taken at exactly the same time.

WZ Sagittae (hereafter WZ Sge) is currently known to be the closest CV (43.5 ± 0.3 pc, see Harrison et al. 2004). It reaches $V \simeq 7$–$8$ during outbursts (e.g., Patterson et al. 2002; Kuulkers et al. 2011); it spends most of the time, however, in a quiescent state characterized by rather modest optical magnitudes in the range 14–16, (e.g., Steeghs et al. 2007; Kuulkers et al. 2011). It has a short orbital period of ≃81.6 min (Krzemiński 1962; Warner 1976). Apart from showing a large outburst amplitude, WZ Sge has also a long outburst recurrence time: it goes into outburst every 20–30 years. In the literature, there are reports of large outbursts of WZ Sge in 1913, 1946, 1978, and 2001 (see, e.g., Mayall 1946; Brosh et al. 1979; Mattei et al. 2001; Godon et al. 2004; Ishioka et al. 2001, and references therein). For a historical record of these observations, we refer to Kuulkers et al. (2011). Several observational campaigns were devoted to the study of the source characteristics in detail during the 2001 outburst (see, e.g., Patterson et al. 2002; Knigge et al. 2002; Long et al. 2003; Sion et al. 2003).

One prominent scenario for the long outburst recurrence time is that the inner part of the accretion disk is truncated by the magnetic field of the white dwarf (see, e.g., Warner 1995; Hameury et al. 1997). In this scenario, the ≃28 s periodic modulation in the optical data (see, for example, Patterson et al. 1998; Lasota et al. 1999) is interpreted as possibly related to the white dwarf spin period. In Sect. 4, however, we discuss a counterargument, suggesting that other scenarios should be considered.

The component masses of WZ Sge are still not well known. The photometric solution of Smak (1993) gives a mass of the white dwarf of $M_{\rm wd} \simeq 0.45\ M_\odot$ and a mass ratio of $q \simeq 0.13$, whereas Spruit & Rutten (1998), who modeled the hot spot at

which the mass stream that is transferred from the companion hits the outer accretion disk, obtain $M_{wd} \simeq 1.2\ M_{\odot}$ and a mass ratio $q \simeq 0.075$. As shown by phase-resolved spectroscopy (Steeghs et al. 2007), the binary system is characterized by a primary white dwarf with mass in the range 0.88 $M_{\odot}$–1.53 $M_{\odot}$ and a low mass companion of 0.078 $M_{\odot}$–0.13 $M_{\odot}$ which is close to the brown dwarf mass threshold. If the mean velocity of absorption lines is interpreted as being due to gravitational red-shift (and one uses the mass-radius relation), then the mass of the primary is inferred to be (0.85 ± 0.04) $M_{\odot}$. In the present work, we use the latter value for the mass of the white dwarf in WZ Sge, whih is 0.85 $M_{\odot}$.

WZ Sge has been intensively observed in the X-ray band. Patterson et al. (1998) described both the ROSAT and ASCA observations (as well as *Einstein* and EXOSAT ones) obtained in quiescence. This analysis was successively re-done by Gün (2005) who reported a quiescent 0.1–2.4 keV flux (as obtained from ROSAT PSPC in 1991) of $\simeq 2.8 \times 10^{-12}$ erg cm$^{-2}$ s$^{-1}$ (corresponding to a luminosity of $\simeq 6.3 \times 10^{29}$ erg s$^{-1}$ for a distance of ≃43.5 pc). In addition, Hasenkopf & Eracleous (2002), reanalyzing a 1996 ASCA observation of WZ Sge, found a 0.5–10 keV flux of $\simeq 4.7 \times 10^{-12}$ erg cm$^{-2}$ s$^{-1}$, which implies a luminosity of $\simeq 1.0 \times 10^{30}$ erg s$^{-1}$. Furthermore, the 2001 outburst of WZ Sge was observed in X-rays (see, e.g., Wheatley et al. 2001; Kuulkers et al. 2006; Wheatley & Mauche 2005).

In this paper, we present the results from ∼9.9 ks *XMM-Newton* measurements and the ∼1.4 ks *Swift* observations of WZ Sge acquired in 2003 and 2011, respectively, which are almost two and ten years after the most recent outburst. The *XMM-Newton* data were already reported by Mukai & Patterson (2004), who used a multi-temperature plasma to describe the observed WZ Sge X-ray spectra and found a 2−10 keV band flux of $\simeq 7.0 \times 10^{-12}$ erg cm$^{-2}$ s$^{-1}$ (i.e., much larger than the flux inferred by using the 1996 ASCA data). We report here on a coherent periodicity of ≃28.96 s in the same *XMM-Newton* observation by using all the information down to 0.2 keV. The detected periodicity is close to that found in the optical reported by Mukai & Patterson 2004.

The paper is structured as follows: In Sects. 2.1 and 2.2, we present the available data and give details about the *XMM-Newton* and *Swift* data reduction, respectively; in Sect. 3 (and related sub-sections), we present the results of our timing and spectral analysis. Finally, we conclude on our observations in Sect. 4.

## 2. Observations and data reduction

### 2.1. XMM-Newton

WZ Sge was observed by *XMM-Newton* (observation ID 0150100101) for ≃9.9 ks starting on 2003 May 16 (14:52:0.7 UT). The target was observed by the three types of X-ray instruments (see, e.g., Jansen et al. 2001): RGS 1 and 2; EPIC-MOS 1 and 2 operating in small window mode, and EPIC-pn in full frame mode; and the Optical Monitor (OM) on board *XMM-Newton*. Here, we concentrate on the analysis of the data acquired by the MOS, pn, and OM cameras.

The observation raw data files (ODFs) were processed using the *XMM*-Science Analysis System (SAS, version 13.0.0) and with up-to-date current calibration files (CCF). The data for the EPIC cameras were processed by running the *emchain* and *epchain* tools, while the *omfchain* pipeline was executed to obtain the optical (background corrected) light curve of WZ Sge. Following the standard screening procedure described in the XRPS User's manual (2008), we extracted light curves above 10 keV for the full MOS and pn cameras. Hence, by identifying and discarding parts of the observation affected by high levels of background activity, the effective observation exposure times resulted in ≃4.3 ks and ≃2.2 ks for the MOS and pn cameras, respectively. While the events collected during the good time intervals were used in the spectral analysis, the timing analysis was performed without applying any time filter as the introduction of gaps may have lead to artifacts.

The *X*-ray emission from the source was extracted from a circular region centered on the nominal position of WZ Sge and with a radius chosen to contain at least 80% of the total source energy. The background signal was extracted from circular regions on the same chip. Finally, the source light curves (one per each EPIC camera) were obtained after subtracting the background counts. We furthermore checked that the resulting data did not show residual effects due to the high energy background. We applied the Solar System barycenter correction, ensuring that the event times were in barycentric dynamical time instead of spacecraft time; the SAS task *epiclccorr* was used to account for absolute and relative corrections.

Following the standard procedures described in the XRPS User's manual (2008), we filtered the event list files of the MOS 1, MOS 2, and pn cameras to exclude any background flare. Here, we adopted the thresholds of 0.3 count s$^{-1}$ and 0.4 count s$^{-1}$ for MOS 1 (MOS 2) and pn, respectively. Then, we accumulated the spectra of the source from a circular region centered on the nominal WZ Sge position, while the spectra of the background were extracted from nearby circular regions. Hence, all the spectra were rebinned to ensure at least 25 counts per energy bin.

The EPIC MOS 1, MOS 2, and pn source light curves were extracted over the energy range 0.3−8 keV with 10 s and 2 s binning; the former were for plotting purposes and the latter for period searching. Finally, the three background-subtracted light curves were combined (averaged) to increase the signal-to-noise ratio.

In addition, the fast mode of the OM telescope allowed us to obtain the UV light curve (in the *UVW1* filter, 200−400 nm) of the source. In the *UVW1* filter, the observed average source magnitude is 13.45 ± 0.06, which corresponds to a quiescent flux of $\simeq 1.57 \times 10^{-14}$ erg cm$^{-2}$ s$^{-1}$ Å$^{-1}$, for the standard Vega magnitude to flux conversion[1].

### 2.2. Swift/XRT

*Swift*/XRT observed the source on three occasions in 2011 November, but we only used the observation taken on 2011 November 14 (10 : 00 : 00 UT; ID 00032125002), which had the longest exposure (≃1.4 ks)[2]. The *Swift* data were analyzed using standard procedures (see Burrows et al. 2005) and the latest calibration files available[3]. In particular, we processed the XRT products with the *xrtpipeline* (v.0.12.6) task, which applied the standard screening criteria by using ftools (Heasoft v.6.13.0) and with the *xselect* task we extracted the source spectra and light

[1] More information on the conversion between OM count rates to magnitude and fluxes is available at http://xmm.esac.esa.int/sas/current/watchout

[2] The other observations, with IDs 00032125001 and 00032125004, have exposure times of only ≃594 s and ≃51 s, respectively.

[3] The latest *Swift* related softwares and calibration files can be found at http://heasarc.nasa.gov/docs7swift/analysis/

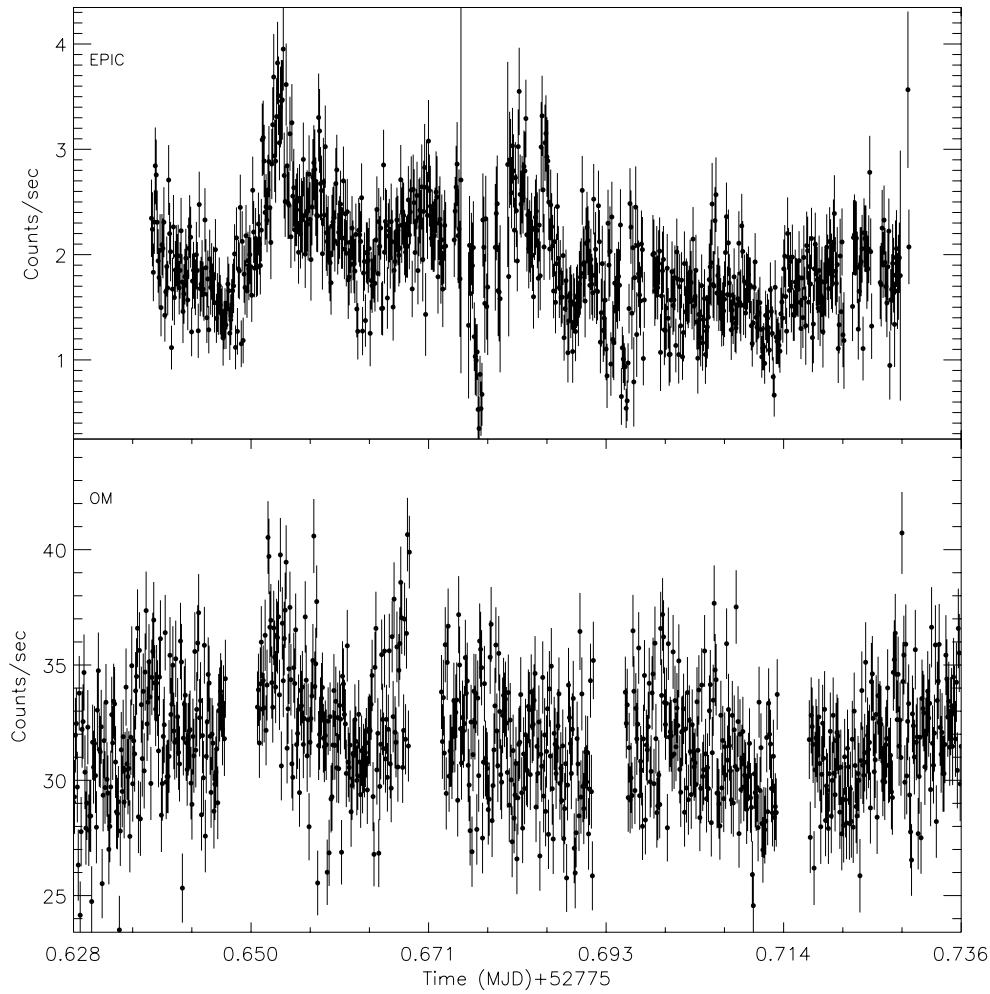


**Fig. 1.** *Upper panel*: 0.3–8 keV *XMM-Newton*/EPIC (averaged) background- and barycentric corrected light curve of WZ Sge with a time resolution of 10 s. *Bottom panel*: OM barycentric corrected light curve with a bin size of 10 s.

curves (in the 0.3−10 keV band) from a circular region (with radius of ≃47″) centered on the target nominal coordinates.

The background spectra and light curves were accumulated from a circular region with the same radius as the source extraction region. We first corrected the source light curve for losses caused by bad columns by using the *xrtlccorr* task, and then we subtracted the background light curve (scaling for the extraction areas) by using the *lcmath* tool. We used the *xrtmkarf* task to generate the ancillary response files and account for different extraction areas of the source and background with regard to vignetting and PSF corrections.

## 3. Analysis and results

### 3.1. *XMM-Newton* temporal analysis results

The MOS 1, MOS 2, and pn single light curves have average count rates of $1.13 \pm 0.87$ count s$^{-1}$, $1.10 \pm 0.86$ count s$^{-1}$, and $3.53 \pm 1.56$ count s$^{-1}$, respectively, while the combined (averaged) background corrected (0.3–8 keV) light curve has an average count rate of $1.92 \pm 0.69$ count s$^{-1}$ per instrument. The combined (MOS and pn averaged) *XMM-Newton*/EPIC light curve is shown in Fig. 1 (upper panel). For comparison, we also present (bottom panel) the OM (*UVW1* filter) light curve of WZ Sge binned at 10 s.

The source is variable on several time-scales and shows structures that may resemble dip features produced by absorbing matter that intervenies along the line of sight (see Sect. 4). To test this hypothesis, we produced background-corrected light curves in the energy ranges 0.3−2.0 keV and 2.0−8.0 keV (soft and hard bands[4], respectively) and define the hardness ratio as the ratio between the hard light curve to the soft one. The result of this approach is given in Fig. 2: the hard and soft light curves are given in the upper and middle panels, respectively, while the hardness ratio is shown in the bottom panel. Inspection of this figure shows that the hardness ratio remains practically constant during the observation, indicating that the photon counts in the soft and hard energy ranges strongly correlate.

When analyzing the 1991 ROSAT PSPC data of WZ Sge in the energy band up to 2 keV by averaging over various orbital cycles, Patterson et al. (1998) found that the soft to hard X-ray ratio (also known as *softness ratio* in the energy bands 0.2 keV−0.4 keV and 0.4 keV−2 keV) clearly showed a

[4] The MOS 1, MOS 2, and pn single light curves in the soft band have average count rates of $0.80 \pm 0.14$ count s$^{-1}$, $0.79 \pm 0.13$ count s$^{-1}$, and $2.68 \pm 0.61$ count s$^{-1}$, respectively. The combined (averaged) 0.3–2 keV light curve has a typical count rate of $1.43 \pm 0.26$ count s$^{-1}$. When the hard band is considered, we find $0.33 \pm 0.27$ count s$^{-1}$, $0.31 \pm 0.25$ count s$^{-1}$, and $0.84 \pm 0.39$ count s$^{-1}$ for the MOS 1, MOS 2, and pn, respectively, while the combined hard light curve has an average count rate of $0.49 \pm 0.18$ count s$^{-1}$.

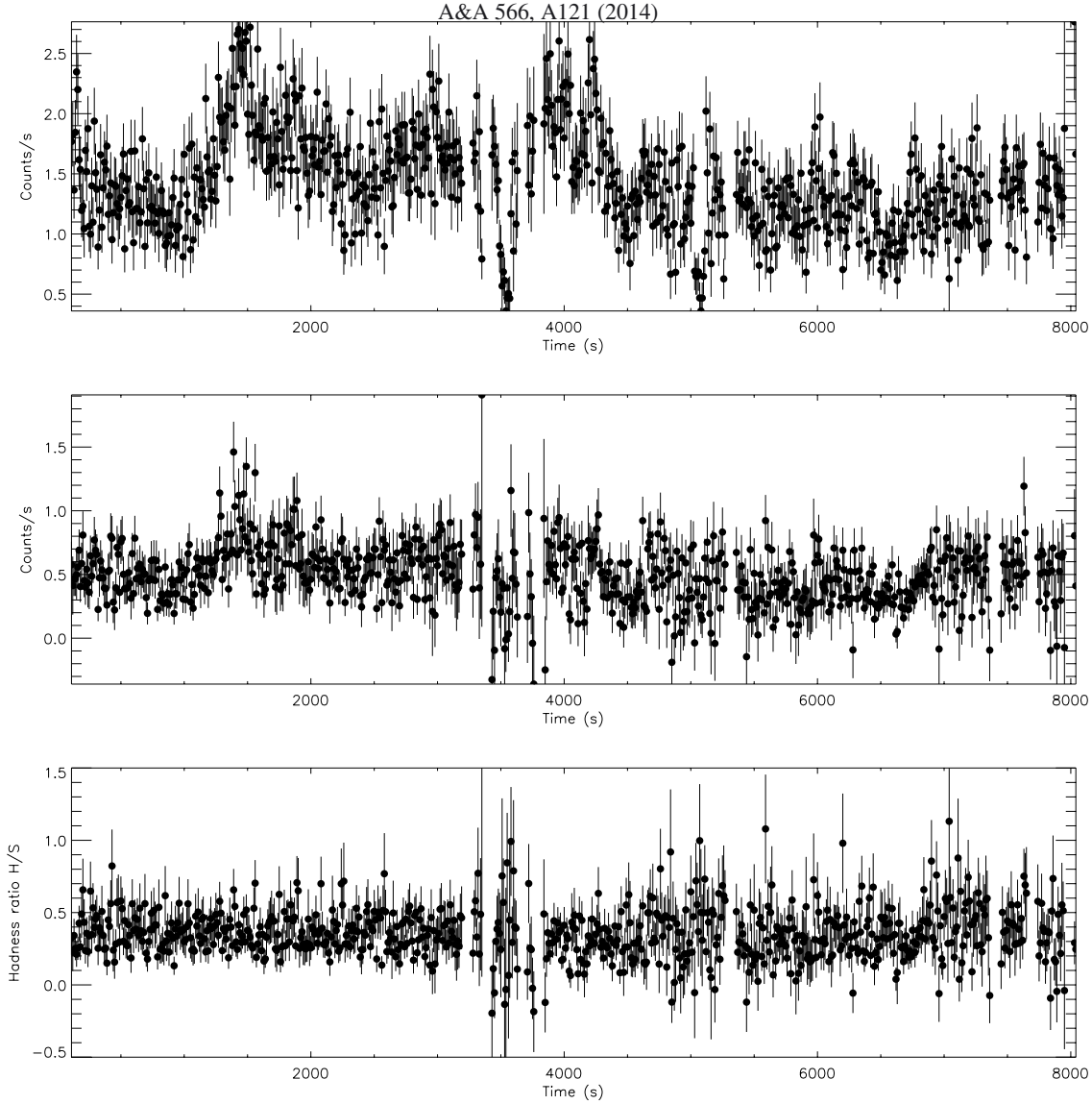


**Fig. 2.** *Upper and middle panels*: light curves (10 s bins) in the soft (0.3−2 keV) and hard (2−8 keV) bands. *Bottom panel*: hardness ratio. For clarity, the time axis is given in seconds with time zero corresponding to the start of the observation.

modulation at the orbital period and a dip at orbital phase ≃0.7. Although we do not have the repeated phase coverage to study the average properties of the dips, we extracted the light curves with a bin size of 240 s corresponding to about 0.05 orbital cycle. The resulting light curves are shown in Fig. 3 (upper panels) with the softness ratio plotted in bottom panel. Here, for convenience, we give the horizontal axes in seconds and in orbital phase by using the ephemeris given in Patterson et al. (1998). The softness ratio has a shape similar to that already observed in the ROSAT PSPC data. In particular the curve shows a modulation at the orbital period, and although not dramatic, a dip appears close to the orbital phase ≃0.7.

We quantified the variability amplitude of the high-energy and optical light curves, using the normalized excess variance ($\sigma^2_{\rm NXS}$, see, e.g., Nandra et al. 1997; and Edelson et al. 2002) and evaluated the associated errors according to Eq. (11) in Vaughan et al. (2003). The result of our analysis is shown in Fig. 4. Here, we give the excess variance for the combined EPIC (upper panel) and OM (bottom panel) light curves (each with a bin size of 10 s) calculated in five (equally spaced) time bins. Since negative values of $\sigma^2_{\rm NXS}$ indicate absence or very small variability in the time series, we conclude that both the high energy and optical data of WZ Sge present a certain degree of intrinsic variability, which seems to vary with time. When we fitted (separately) each normalized excess variance with a linear function (represented in both panels of Fig. 4 by the dashed lines), we found that the rate of change in time of $\sigma^2_{\rm NXS}$ for the X-ray and optical data is $\simeq -4.4 \times 10^{-6}$ and $\simeq -2.4 \times 10^{-7}$, respectively.

We blindly searched for periodicities in the time range from 2 s to a few hours in the X-ray light curve by applying the Lomb-Scargle technique (Lomb 1976; Scargle 1982). In particular, we used $\nu_{\rm min} = 1/(3T_{\rm obs})$ and $\nu_{\rm max} = 1/(2\delta t)$ with $T_{\rm obs}$, the duration of the observation, and $\delta t$, the associated time step, as the minimum and maximum values of the frequency range to be searched for periodicity. Using the minimum frequency $\nu_{\rm min}$, we note we implicitly require at least three full cycles per observational window. The analysis resulted in the periodogram shown in Fig. 5. In the upper panel, we show the periodogram in the period range of 10−100 s, while we show the periodogram in the range 100−2600 s in the bottom panel. The significance of each peak appearing in the periodogram was evaluated by following the recipe described by Lomb (1976); Scargle (1982). In particular, we compared the height of each peak with the power threshold that corresponds to a given false alarm probability in

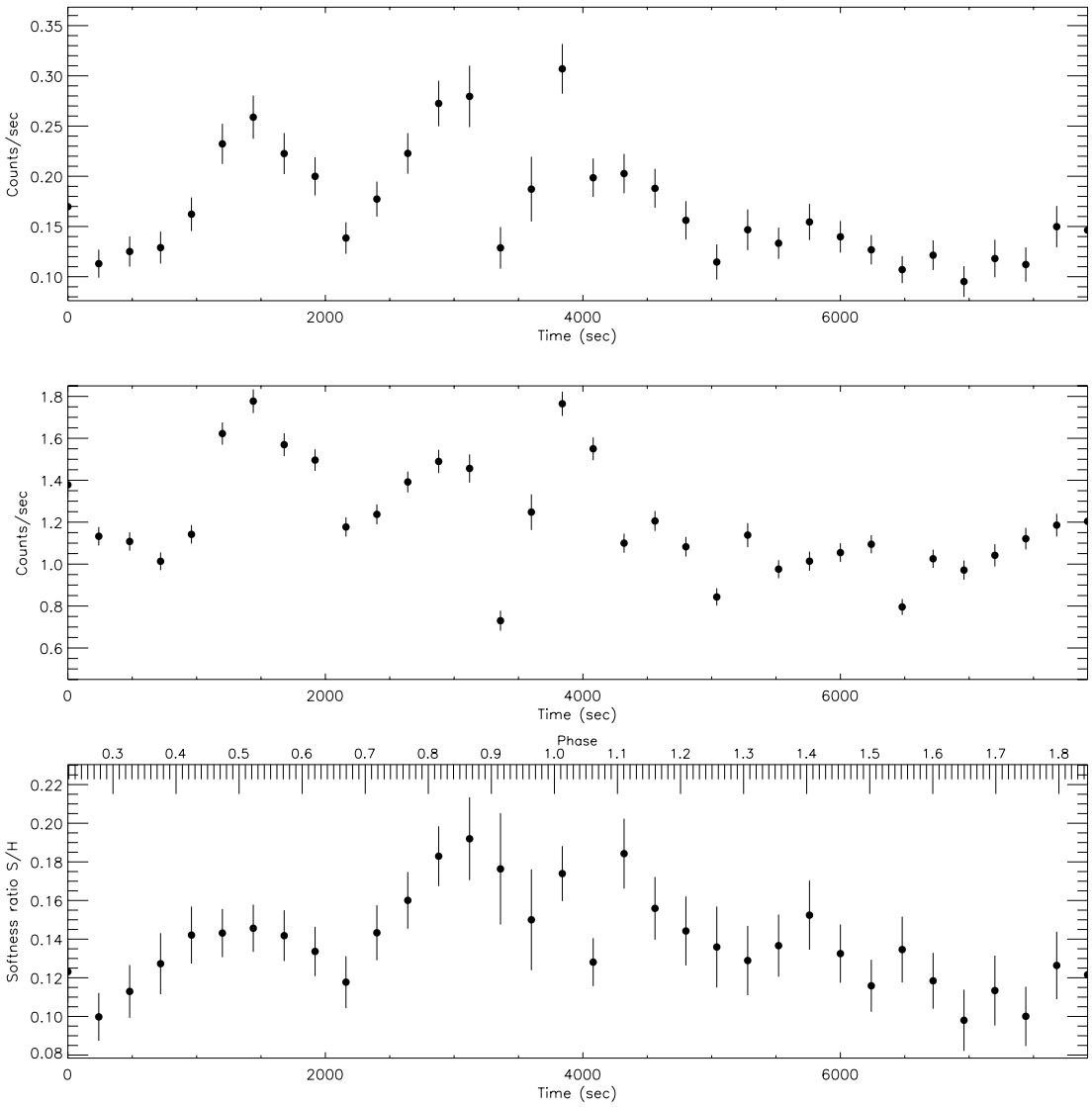


**Fig. 3.** WZ Sge light curves between 0.2 keV and 0.4 keV (*upper panel*) and between 0.4 and 2 keV (*middle panel*). *Bottom panel*: softness ratio (see text for details).

white noise simulations: the three horizontal lines given in Fig. 5 correspond to false alarm probability thresholds of 68% (solid line), 90% (dotted line), and 99% (dashed line), respectively.

It is clear that we detect a periodicity of $28.96^{+0.02}_{-0.01}$ s in the 0.3−8 keV light curve (Fig. 5, upper panel), as it is the $1\sigma$ error on the detected period that is estimated with the technique described in Carpano et al. (2007). This period was confirmed (within the quoted error range) by using the epoch folding method. In particular, we iteratively folded the light curve at a trial period $P$, fitted the resulting light curve with a sine function and searched for the period that minimized the $\chi^2$ statistics. The period is consistent with the low significance signal reported by Mukai & Patterson (2004) when analyzing the same set of *XMM-Newton* data in the 2−10 keV energy band and the coherent periodicity detected in 2003 in the MDM 2.4 m telescope data by the same authors. In accordance with Mukai & Patterson (2004) we confirm that the 28.96 s peak becomes less significant when we consider the light curve in the 2−10 keV band. Moreover, we do not detect any coherent period at ≃27.87 s, which is the presumed spin period of the white dwarf (see Sect. 1).

In the bottom panel of Fig. 5, we show the Lomb-Scargle periodogram in the period of range 100−2600 s. Note that the features appearing at ≃1400 might be associated to longer timescales that is present in the light curves.

We folded the EPIC light curve and the hardness ratio curve on the 28.96 s period with 15 bins and 8 bins per cycle, respectively. The result is shown in Fig. 6. The solid line in the upper panel corresponds to a sinusoidal fit[5] to the data having $\chi^2 = 0.8$ for 26 degrees of freedom (d.o.f.): in particular, the amplitude of the sine signal is $A = 0.09 \pm 0.01$ count s$^{-1}$. In the bottom panel, the solid and dashed lines represent a sinusoidal (with amplitude $A = 0.017 \pm 0.003$ and $\chi^2 = 0.14$ for 12 d.o.f.) and linear (with constant value of $C = 0.34 \pm 0.01$ with $\chi^2 = 0.5$ for 13 d.o.f.) fits to the folded hardness ratio. As it is evident, the hardness ratio data is consistent with being constant in time although it appears to show a low modulation by eye.

We applied the same procedure to the OM light curve (see Fig. 7). We do not detect the coherent period at ≃28.96 s nor the

[5] We performed the sinusoidal fit with the function $s(t) = A\sin(2\pi\phi + B) + C$, where $\phi$ is the phase and $A$, $B$ and $C$ are the free parameters.

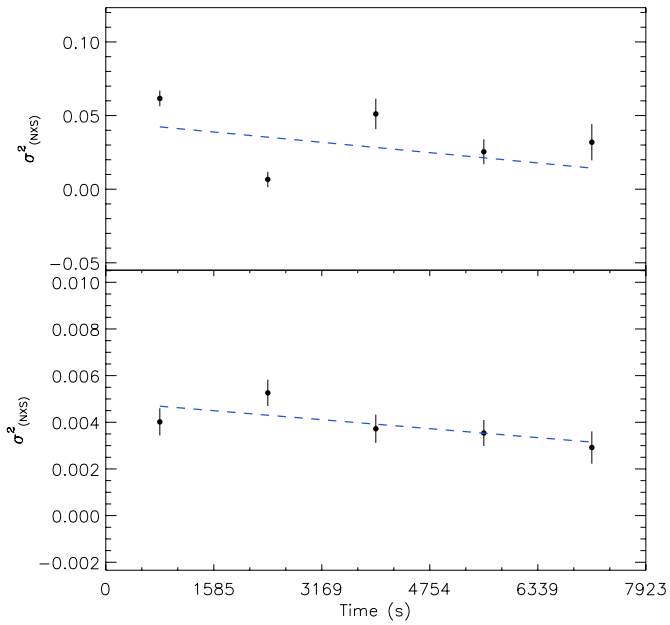


**Fig. 4.** Excess variance, $\sigma^2_{NXS}$, of the combined EPIC (*upper panel*) and OM (ıbottom panel) light curves of WZ Sge (see text for details).

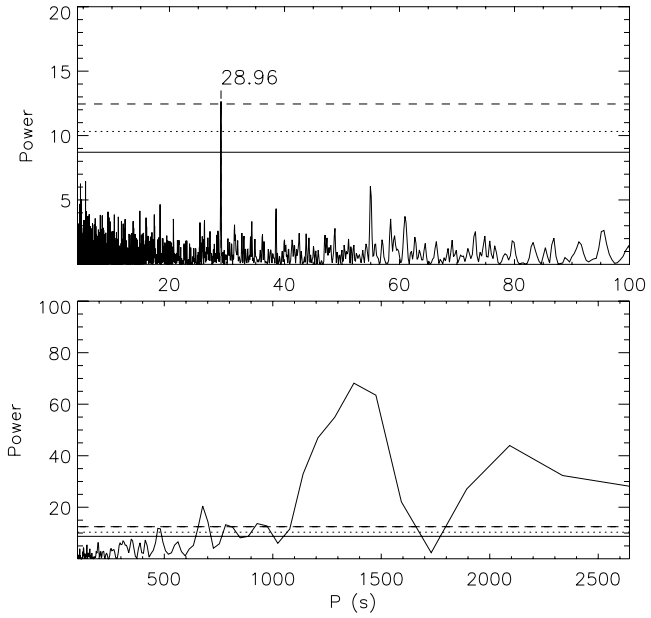


**Fig. 5.** Lomb-Scargle periodogram of the WZ Sge combined EPIC light curve in the 0.3−8 keV band (see text for details).

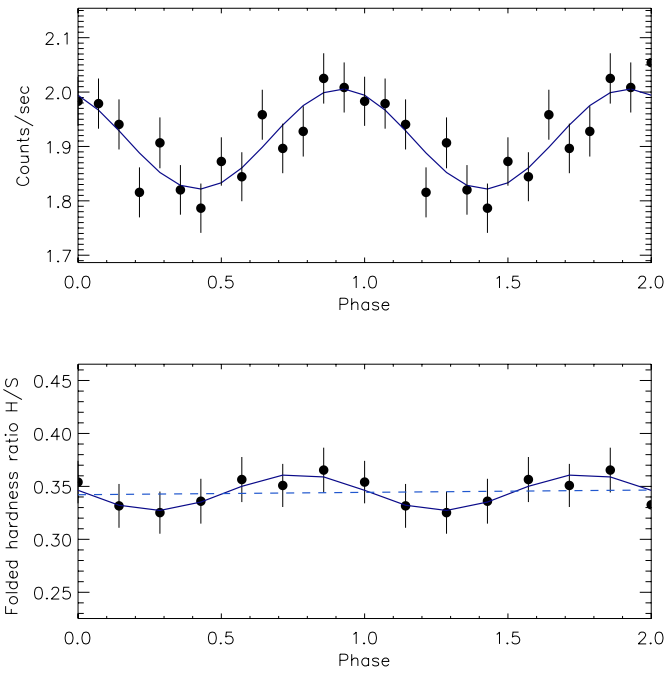


**Fig. 6.** High-energy light curve of WZ Sge (0.3−8 keV; *upper panel*) and the hardness ratio (*lower panel*) folded at ≃28.96 s with 15 bins and 8 bins per cycle, respectively. See text for details.

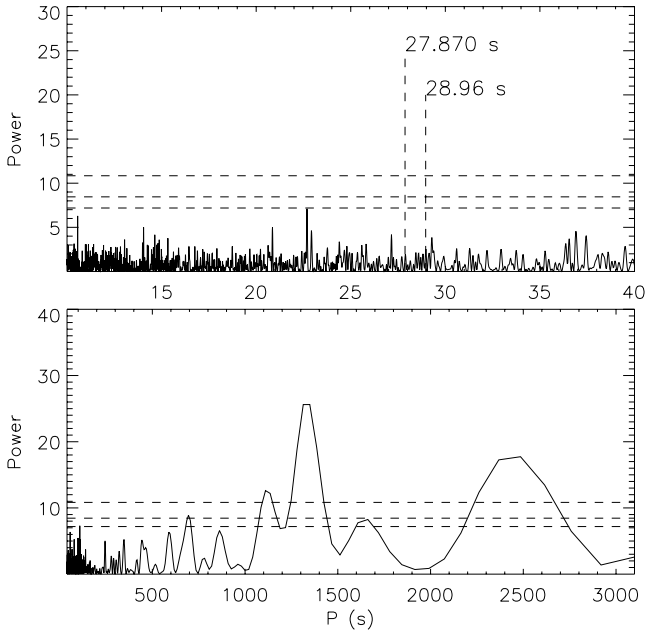


**Fig. 7.** Same as in Fig. 5 for the OM data of WZ Sge.

periodicity of ≃27.87 s. We also verified with a phase resolved periodogram that the peak appearing at ≃22 s is not significant.

### 3.2. Swift/XRT temporal analysis results

The quality of the 2011 *Swift*/XRT data do not allow us to perform a detailed timing analysis similar to the *XMM-Newton* data set: the observed *Swift*/XRT average count rate is ≃0.14 count s$^{-1}$ during ≃1.4 ks. We obtained the quiescent WZ Sge light curve in the 0.3−10 keV energy band with a bin size of 50 s, which is shown in Fig. 8. Over the course of the observation, we do not see significant variability.

### 3.3. XMM-Newton and Swift/XRT X-ray spectral analysis

The *XMM-Newton* and *Swift*/XRT source spectra (including the response matrices, ancillary files, and background spectra) were read into the XSPEC package (version 12.4.0) for the spectral analysis and fitting procedure. A first fit attempt showed that the spectral shape of the source did not change significantly between the times of the *XMM-Newton* and *Swift*/XRT observations. Hence, we fitted the data with all the model parameters linked together, apart from a multiplicative dimensionless constant, which can take different values for the *XMM-Newton* and *Swift*/XRT spectra. The multiplicative factor mostly accounts for

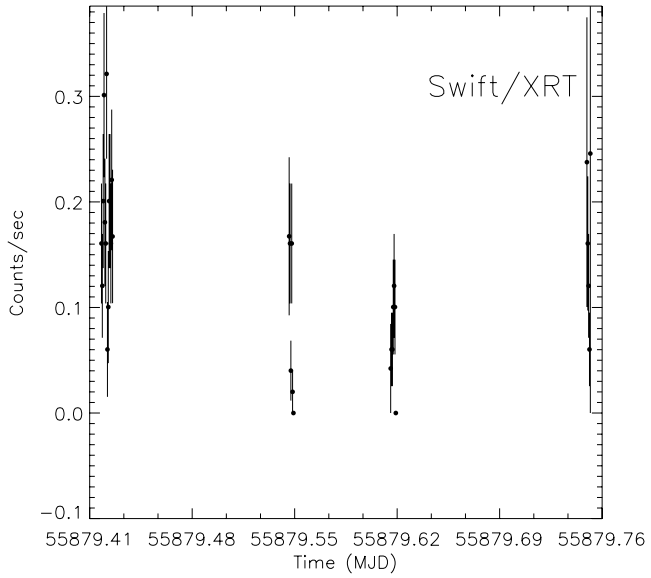


**Fig. 8.** *Swift*/XRT light curve of WZ Sge in the 0.3−10 keV energy band with a time bin size of 50 s.

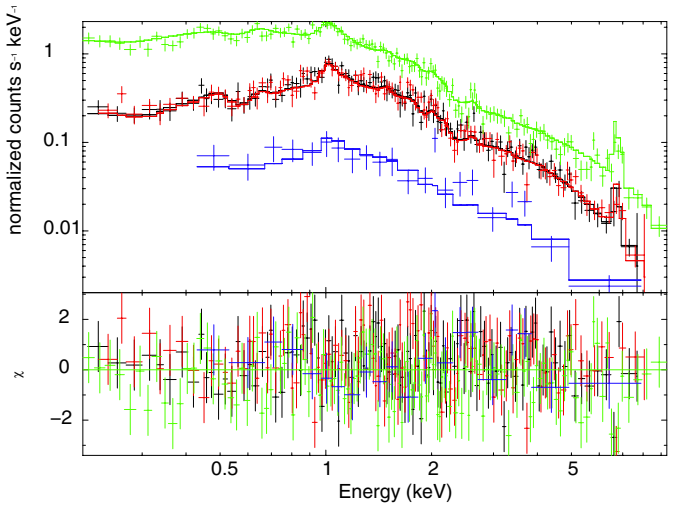


**Fig. 9.** *Upper panel*: MOS (black and red crosses), pn (green crosses) and XRT (blue crosses) spectra together with the best-fit model (solid lines). *Bottom panel*: residuals between data and the best-fit model.

any flux change of the source that might have happened between the two observations.

Without success, we tried to fit the spectra by using a single thermal plasma component absorbed by neutral gas (Mekal and Phabs in XSPEC). Fixing the hydrogen column density to the average value[6] found in the direction of the target ($n_{\rm H} \simeq 2 \times 10^{21}$ cm$^{-2}$, Dickey & Lockman 1990) and/or allowing the metallicity abundance to vary did not improve our fit significantly. In particular, we noted the existence of residuals at low energies around the iron L-shell complex at ≃1 keV. These kind of residuals may be due to two effects: the improper modeling of photo-electric absorption and the fluorescence from cold material with a multi-temperature structure of the spectrum (see, e.g., Baskill et al. 2005). To account for such a line, we added an extra Gaussian component (Gauss in XSPEC). Thus, our model, K*phabs(mekal + gaussian), consists of seven free parameters, i.e., the hydrogen column density $n_{\rm H}$ toward the source; the plasma temperature $kT$; the normalization $N$ of the emission model; the position $E$, the width $\sigma_E$, and the normalization $N_E$ of the Gaussian line; the multiplicative constant $K$, which accounts for any difference in flux among the spectra from the different instruments. We fixed $K$ to 1 for the *XMM-Newton*/MOS 1, MOS 2, and pn spectra while we allowed it to vary for the *Swift*/XRT data. The other parameters of the *Mekal* model, which the solar abundance and hydrogen number density, were fixed to the respective default values.

Using the above model, we obtained $N_{\rm H} = (0.031 \pm 0.004) \times 10^{22}$ cm$^{-2}$, $KT = 6.9 \pm 0.5$ keV, $N = (5.5 \pm 0.1) \times 10^{-3}$, $E = 1.01^{+0.01}_{-0.02}$ keV, $\sigma_E \lesssim 0.07$ keV, $N_E = (9.6^{+3.0}_{-2.0}) \times 10^{-5}$ (with $\chi^2 = 1.24$ for 393 d.o.f.). Based on the multiplicative factor, we find that the *Swift*/XRT data show an overall decrease in flux by a factor $K = 0.59 \pm 0.07$ as determined by our best fitting procedure.

The Gaussian line at ≃1 keV may be due to the L-shell complex or to the H-like line of Ne expected around this energy. Hence, we tried to fit the data with a more physical model consisting of a two-temperature plasma model. The best fit procedure resulted ($\chi^2 = 1.16$ for 394 d.o.f.) in a hydrogen column density formally consistent with the value quoted above and plasma temperatures of $KT_1 = 9.04^{+1.15}_{-0.91}$ keV and $KT_2 = 1.31^{+0.08}_{-0.13}$ keV with normalizations $N_1 = (5.0 \pm 0.1) \times 10^{-3}$ and $N_2 = (4.9 \pm 0.1) \times 10^{-3}$, respectively. Also in this case, the *Swift*/XRT data show a flux decrease by a factor $K = 0.59 \pm 0.07$.

In Fig. 9, we present the MOS 1, MOS 2, pn, and XRT spectral data in the energy band 0.2−10.0 keV with the two-temperature best-fit model. The total absorbed flux in the 0.2−10.0 keV band is $F^{\rm Abs}_{0.2-10.0} = (1.09 \pm 0.02) \times 10^{-11}$ erg s$^{-1}$ cm$^{-2}$ for the *XMM-Newton* 2003 observation (i.e., consistent with what found by Mukai & Patterson 2004) and $F^{\rm Abs}_{0.2-10.0} = (6.47^{+0.69}_{-0.74}) \times 10^{-12}$ erg s$^{-1}$ cm$^{-2}$ for the *Swift* 2011 observation. The errors quoted are at the 90% confidence level. As noted by Mukai & Patterson (2004), the 2003 WZ Sge flux (restricted to the 2−10 keV energy band) is higher than the 1996 May ASCA data (≃$2.9 \times 10^{-12}$ erg s$^{-1}$ cm$^{-2}$). The 2011 *Swift* data show that the high-energy signal returned to a similar level to that observed in 1996 which preceded the last source outburst.

Assuming a distance of 43.5 ± 0.3 pc (see, e.g., Harrison et al. 2004), the X-ray luminosity of WZ Sge in 2003 was $L^{\rm Abs}_X = (2.47 \pm 0.06) \times 10^{30}$ erg s$^{-1}$, while in 2011 it was $L^{\rm Abs}_X = (1.41^{+0.17}_{-0.16}) \times 10^{30}$ erg s$^{-1}$ in 2011. The major contribution to the error in the luminosity comes from the error associated to the source distance. Correcting for the absorption, we get an intrinsic luminosity of $L^{\rm Una}_X = (2.65 \pm 0.06) \times 10^{30}$ erg s$^{-1}$ and $L^{\rm Una}_X = (1.57^{+0.18}_{-0.17}) \times 10^{30}$ erg s$^{-1}$ in 2003 and 2011, respectively.

## 4. Discussion

### 4.1. Quiescent X-rays

In this paper, we presented the analysis of an archival *XMM-Newton* observation in 2003 (for a preliminar study, see Mukai & Patterson 2004) and newly acquired *Swift* data in 2011 of WZ Sge.

WZ Sge's X-ray spectral properties in the 0.2−10 keV energy band remained practically unchanged between the 2003 and 2011 observations. We estimated an unabsorbed intrinsic luminosity of $L^{\rm Una}_X = (2.65 \pm 0.06) \times 10^{30}$ erg s$^{-1}$ and

[6] See the online calculator available at http://heasarc.gsfc.nasa.gov/cgi-bin/Tools/w3nh/w3nh.pl which gives the integrated neutral hydrogen column density through the Galaxy.

$L_X^{\rm Una} = (1.57 \pm 0.03) \times 10^{30}$ erg s$^{-1}$ for the 2003 and 2011 observations, respectively. The luminosity in 2011 is a factor ≃2 lower than that in 2003, indicating that WZ Sge returned to a level similar to that observed prior to the last source outburst in 2001.

The high-energy light curves confirm the existence of a dip close to the orbital phase ≃0.7. Although this feature is not strong, it also appears in the softness ratio light curve, similar to that seen using ROSAT/PSPC data (Patterson et al. 1998). Dip structures in the light curves are naturally explained in the framework depicted by Frank et al. (1987, see also Krzemiński & Smak 1971) which is supported by the numerical simulation of Hirose et al. (1991) and Armitage & Livio (1998). The model found its application in explaining periodic orbital dip features in the high-energy light curves of nova-like systems (see e.g., Hoard et al. 2010 and Nucita et al. 2011) and of magnetic white dwarfs (see Ramsay et al. 2009). According to this model, once the mass flow reaches the inferior conjunction at the orbital phase 0.7, part of the accreting matter sets sufficiently high above the disk, thus obscuring the white dwarf and producing the observed dip.

### 4.2. Periodicities at 27.87 and 28.96 s

With an improved analysis (using all the available data down to 0.2 keV), we find a coherent periodicity of ≃28.96 s in the 2003 observation. This confirms the weak detection reported by Mukai & Patterson (2004); the period is close to that found in optical data reported by the same authors. We did not detect the 27.87 s oscillation attributed to the white dwarf spin (see, e.g., Patterson et al. 1998; Lasota et al. 1999), similar to Mukai & Patterson (2004).

The origin of the 27.87 s and the 28.96 s periods in WZ Sge has been a long-standing puzzle. For example, Robinson et al. 1978 interpreted these two distinct periods as due to non-radial pulsations. Patterson et al. (1998) cautiously argued that the 27.87 s period seen in the ASCA X-ray data was the spin period of a magnetic white dwarf. Welsh et al. (2003) presented a balanced review of the two models and pointed out the difficulties with both. Given that ten years have elapsed since then, during which a large body of recent observations of non-radial pulsations in other low-accretion rate dwarf novae have been obtained, we present a re-assessment of the models.

Lasota et al. (1999) proposed that the 27.87 s is the white dwarf spin period, while the 28.96 s signal is due to reprocessing of the spin signal by a blob at the outer rim of the Keplerian disk. While this explanation is viable for an *optical* modulation at the 28.96 s period, it fails to explain the 28.96 s X-ray period. While intermediate polars often show X-ray spin and sideband signals simultaneously (Norton et al. 1996), this is believed to be due to stream overflow, which is a mass transfer stream that skirts the surface of the disk and is directly captured by the magnetic field of the white dwarf. It is hard to see how the white dwarf can accrete directly from a blob at the outer edge of the disk. If, instead, the Keplerian period at the inner edge of the disk is 733.5 s (see, however, objections to this idea by Lasota et al. 1999), this could in principle lead to an X-ray modulation at the 28.96 speriod. In this case, however, it would be difficult to avoid a strong X-ray modulation at the 733.5 s period (Wynn & King 1992), given the high inclination of the WZ Sge system. That is, when the blob that feeds the magnetic pole is on the Earth side of the white dwarf, the pole that is facing the Earth would accrete more favorably. This is likely to lead to a higher observed X-ray flux than when the blob is on the far side. In addition, both the inner and outer radii of an accretion disk are not constant when the accretion rate varies; it is not clear how a blob with a Keplerian period of 733.5 s is always favored, when both the optical (Kuulkers et al. 2011) and the X-ray (this work) brightness show secular variability.

Further arguments against an intermediate polar model come from the hardness curves. We do not find any evidence for X-ray spectral variations along the 28.96 s signal. Usually, the X-ray emission is softer when brighter in intermediate polars. We note that, indeed, WZ Sge is not classified as a standard member of this class of objects (see, e.g., Knigge et al. 2002).

The above described weaknesses, however, may not be fatal for the magnetic CV model of the twin periods. Nevertheless, the *XMM-Newton* detection of the 28.96 s signal makes the argument that the 27.87 s period is the spin period of a magnetic white dwarf somewhat weaker.

There is little doubt that the short period variability seen in another faint CV, GW Lib (see also below), is due to non-radial g-mode pulsations of the white dwarf that dominates its optical light in quiescence (van Zyl et al. 2004). Since then, similar pulsations have been discovered in about a dozen of other faint, white dwarf-dominated CVs (see, e.g., Szkody et al. 2010, and references therein). In the case of these accreting white dwarfs, which are rapidly rotating and have peculiar abundances, these pulsations are more complicated than in the non-accreting ZZ Cet stars. For example, CV primaries may show pulsations outside the ZZ Ceti instability strip. The <30 s periods in WZ Sge, however, are significantly shorter than those seen in GW Lib type CVs (>200 s). Moreover, X-rays are generated by accretion, and it is not clear how non-radial pulsations would modulate the X-ray flux.

In summary, the origin of the twin pulsations is as mysterious as ever. The long-term stability of the intermittent 27.87 s period remains the strongest argument for this to be the spin period of the white dwarf, but this leaves us without a clear understanding of the 28.96 s period. It is interesting to note that Mukadam et al. (2013) found several puzzling features in the pulsational variability of another CV, EQ Lyn. In addition to possible ways to reconcile these observations with our understanding of g-mode pulsations, they considered alternatives models: r-mode pulsations and accretion disk pulsations. We should possibly keep in mind such alternative possibilities when considering WZ Sge.

### 4.3. On the quiescent rate of accretion

In addition to the twin periods of 27.87 s and 28.97 s, WZ Sge possesses several characteristics that made it stand out among dwarf novae. These include the short orbital period, the quiescent spectrum, which is dominated by the white dwarf photosphere, the large outburst amplitude, and the long inter-outburst interval. However, recent advances show that CVs with many of these latter characteristics are quite common. In particular, the Sloan survey has revealed a large population of CVs near the period minimum ($P$ < 88 min), whose spectra are often dominated by the white dwarf photosphere (Gänsicke et al. 2009). The earlier surveys did not go deep enough to show the prevalence of this population. Many of these newly discovered systems are candidate WZ Sge stars in terms of their outburst characteristics; they are generally seen in a quiescent dwarf nova-like state since their discovery, so any outbursts must be infrequent.

The best studied such system is the aforementioned CV, GW Lib, whose discovery predated the Sloan survey. Its well-documented 2007 outburst (Byckling et al. 2009; Vican et al. 2011) is the second known after the discovery outburst in 1983.

It has a 76.8 min orbital period, its quiescent spectrum is dominated by the white dwarf photosphere, the outburst amplitude is large (~9 mag), and its duration long (~26 day). Surely, GW Lib presents a similar challenge to the disk instability model that WZ Sge does. Yet, despite intensive observations motivated by its status as the prototype CV with non-radial pulsations, no spin-period signature has ever been observed in GW Lib.

Of the many systems that share various degrees of similarity with WZ Sge (Gänsicke et al. 2009), only V455 And (HS 2331+3905; Araujo-Betancor et al. 2005) is known to be magnetic. Intensive searches for additional non-radial pulsators have not led to discoveries of magnetic CV signatures among other WZ Sge-like systems. Unless all systems near the period minimum are sufficiently magnetic to create a hole in the disk and somehow manage to hide any spin signatures, we must seek an explanation for the long interval, long duration, and large amplitude outbursts that do not rely on the primary's magnetic field. In particular, if the correlation found by Patterson (2011) between the outburst recurrence time and the mass ratio is confirmed, some factor directly related to the mass ratio is strongly implied as the cause of the long recurrence time in WZ Sge type systems; the magnetic field of the white dwarf would be a second parameter, not the primary.

If that is the case, the twin periods of WZ Sge, whatever their origin, may well be a red herring in terms of understanding the outburst properties of WZ Sge. For example, while the detailed propeller model of Matthews et al. (2007) can still explain WZ Sge, it fails to explain GW Lib, whose outburst properties are similar to those of WZ Sge. On a possibly related note, the X-ray luminosity of WZ Sge is low compared to dwarf novae with frequent outbursts (U Gem and SU UMa types; Byckling et al. 2010), while it is higher than that of GW Lib or the Sloan-selected systems studied by Reis et al. (2013). Given this, future studies should strive to understand why the quiescent accretion rate in WZ Sge is high compared to other WZ Sge systems and not why it is lower than in normal dwarf novae.

*Acknowledgements.* K.M. thanks Paula Szkody for informative discussion on the latest results of pulsations in low accretion rate CVs. This paper is based on observations from *XMM-Newton*, an ESA science mission with instruments and contributions directly funded by ESA Member States and NASA. Part of this work is based on archival data, software or online services provided by the ASI Science Data Center (ASDC), Italy. We are also in debt with the anonymous referee for pointing us a problem in the *Swift* analysis.

## References

Araujo-Betancor, S., Gänsicke, B. T., Hagen, H.-J., et al. 2005, A&A, 430, 629
Armitage, P. J., & Livio, M. 1998, ApJ, 470, 1024
Baskill, D. S., Wheatley, P. J., & Osborne, J. P. 2005, MNRAS, 357, 626
Brosch, N. 1979, IBVS, 1693, 1
Burrows, D. N., Hill, J. E., Nousek, J. A., et al. 2005, Space Sci. Rev., 120, 165
Byckling, K., Osborne, J. P., Wheatley, P. J., et al. 2009, MNRAS, 399, 1576
Byckling, K., Mukai, K., Thorstensen, J. R., & Osborne, J. P. 2010, MNRAS, 408, 2298
Carpano, S., Pollock, A. M. T., Prestwich, A., et al. 2007, A&A, 466, L17
Dickey, J. M., & Lockman, F. J. 1990, ARA&A, 28, 215
Edelson, R. A., Turner, T. J., Pounds, K., et al. 2002, ApJ, 568, 610
Frank, J., King, A. R., & Lasota, J.-P. 1987, A&A, 178, 137
Gänsicke, B. T., Dillon, M., Southworth, J., et al. 2009, MNRAS, 397, 2170
Godon, P., Sion, E. M., Cheng, F., et al. 2004, ApJ, 602, 336
Gün, G. I. 2005, Int. J. Mod. Phys., 14, 1185
Hameury, J. M., Lasota, J. P., & Hure, J. M. 1997, MNRAS, 287, 937
Harrison, T. E., Johnson, J. J., McArthur, B. E., et al. 2004, AJ, 127, 460
Hasenkopf, C. A., & Eracleous, M. 2002, BAAS, 201, 12003
Hirose, M., Osaki, Y., & Mineshige, S. 1991, PASP, 43, 809
Hoard, D. W., Ting-Ni, Lu., Knigge, C., et al. 2010, AJ, 140, 1313
Ishioka, R., Uemura, M., Matsumoto, K., et al. 2001, IAU Circ., 7669, 1
Jansen, F., Lumb, D., Altieri, B., et al. 2001, A&A, 365, L1
Knigge, C., Hynes, R. I., Steeghs, D., et al. 2002, ApJ, 580, L151
Krzemiński, W., & Smak, J. 1971, Acta Astron., 21, 133
Kuulkers, E., Knigge, C., Steeghs, D., Wheatley, P. J., & Long, K. S. 2002, in The Physics of Cataclysmic Variables and Related Objects, eds. B.T. Gänsicke, K. Beuermann, & K. Reinsch, ASP Conf. Ser., 261, 443
Kuulkers, E., Norton, A., Schwope, A., & Warner, B. 2006, in Compact Stellar X-ray Sources, eds. W. H. G. Lewin, & M. van der Klis, Cambridge Astrophysics Series (Cambridge: Cambridge University Press), 39, 421
Kuulkers, E., Henden, A. A., Honeycutt, R. K., et al. 2011, A&A, 528, A152
Lamb, D. Q. 1982, Cataclysmic Variables and Related Objects: proceeding of the 72nd colloquium of the international astronomical union, eds. M. Livio, & G. Shaviv
Lasota, J. P., Kuulkers, E., & Charles, P. 1999, MNRAS, 305, 473
Lomb, N. R. 1976, Ap&SS, 39, 447
Long, K. S., Froning, C. S., Gänsicke, B., et al. 2003, ApJ, 591, 1172
Mattei, J., Poyner, G., Reszelski, M., et al. 2001, IAU Circ., 7669, 2
Matthews, O. M., Speith, R., Wynn, G. A., & West, R. G. 2007, MNRAS, 375, 105
Mayall, M. W. 1946, Harvard Coll. Obs. Bull., 1918, 3
Mukadam, A. S., Townsley, D. M., Szkody, P., et al. 2013, AJ, 146, A54
Mukai, K., & Patterson, J. 2004, in IAU Coll. 194, eds. G. Tovmassian, & E. Sion, Rev. Mex. Astron. Astrofis., 20, 244
Nandra, K., George, I. M., Mushotzky, R. F., Turner, T. J., & Yaqoob, T. 1997, ApJ, 476, 70
Norton, A. J., Beardmore, A. P., & Taylor, P. 1996, MNRAS, 280, 937
Nucita, A. A., Kuulkers, E., Maiolo, B. M. T., et al. 2011, A&A, 536, A75
Patterson, J. 2011, MNRAS, 411, 2695
Patterson, J., Richman, H., Kemp, J., & Mukai, K. 1998, PASP, 110, 403
Patterson, J., Masi, G., Richmond, M. W., et al. 2002, PASP, 114, 721
Ramsay, G., Rosen, S., Hakala, P., Crdova, F., & Barclay, T. 2009, MNRAS, 395, 416
Reis, R. C., Wheatley, P. J., Gänsicke, B. T., & Osborne, J. P. 2013, MNRAS, 430, 1994
Robinson, E. L., Nather, R. E., & Patterson, J. 1978, ApJ, 219, 168
Scargle, J. D. 1982, ApJ, 263, 835
Sion, E. M., Gänsicke, B. T., Long, K. S., et al. 2003, ApJ, 591, 1137
Szkody, P., Ukadam, A., Gaensicke, B. T., et al. 2010, ApJ, 710, 64
Smak, J. I. 1993, Acta. Astron., 34, 93
Spruit, H. C., & Rutten, R. G. M. 1998, A&A, 335, 227
Steeghs, D., Howell, S. B., knigge, C., & Gänsicke, B. T. 2007, ApJ, 667, 442
Vaughan, S., Edelson, R., Warwick, R. S., & Uttly, P. 2003, MNRAS, 345, 1271
Vican, L., Patterson, J., Allen, W., et al. 2011, PASP, 123, 1156
van Zyl, L., Warner, B., O'Donoghue, D., et al. 2004, MNRAS, 350, 307
Warner, B. 1995, in Cataclysmic Variable Stars, Cambridge Astrophysics Series (Cambridge: Cambridge University Press), 28
Welsh, W. F., Sion, E. M., Godon, P., et al. 2003, ApJ, 599, 509
Wheatley, P. J., & Mauche, C. W. 2005, in The Astrophysics of Cataclysmic Variables and Related Objects, eds. J. M. Bhameuty, & J. P. Lasota, ASP Conf. Ser. (San Francisco: ASP), 330
Wheatley, P. J., Kuulkers, E., Drake, J. J., et al. 2001, IAU Circ., 7677, 1
Wynn, G. A., & King, A. R. 1992, MNRAS, 255, 83
XRPS user's manual 2008, Issue 2.6, eds. M. Ehle, et al.